

Effect of VO_x Species and Support on Coke Formation and Catalyst Stability in Nonoxidative Propane Dehydrogenation

Sergey Sokolov,^[a] Victor Yu. Bychkov,^[b] Mariana Stoyanova,^[a] Uwe Rodemerck,^[a] Ursula Bentrup,^[a] David Linke,^[a] Yuriy P. Tyulenin,^[b] Vladimir N. Korchak,^[b] and Evgenii V. Kondratenko*^[a]

VO_x/SiO₂-Al₂O₃ catalysts were prepared by grafting vanadyl acetylacetonate onto the supports with a SiO₂ content between 0 and 100 wt.%. The degree of polymerization of VO_x species and acidity both of pristine supports and the catalysts were evaluated. To determine their on-stream stability and carbon deposition activity in nonoxidative propane dehydrogenation, continuous-flow tests and in situ thermogravimetric measurements were performed. The rate constants of catalyst

deactivation and carbon deposition were derived from kinetic evaluation of these experiments. Gathered experimental evidence pointed out that VO_x species were significantly more active for coke formation than acid sites of the supports. The rate constant of carbon formation was found to increase with the degree of polymerization of VO_x species, whereas no correlation between catalyst acidity and the rate constants of coking or deactivation could be drawn.

Introduction

Propylene is the second important building block of the chemical industry after ethylene and finds its application in production of polymers, fibers, resins, and solvents. It is industrially produced as a co-product of steam cracking of naphtha and fluid catalytic cracking of heavy oil fractions.^[1,2] Metathesis of ethylene with 2-butenes^[3] and nonoxidative dehydrogenation (DH) of propane^[2] are two commercially available on-purpose propylene production alternatives. Growing extraction of shale gas drives the price of propane down thus making the latter process more commercially attractive despite high energy demand caused by strong endothermicity of the reaction. The existing industrial DH processes employ catalysts based on chromium oxide or metallic platinum.^[2,4] Supported VO_x-containing catalysts were extensively studied for their activity and selectivity in the conversion of C₃-C₄ hydrocarbons into corresponding olefins in the absence of gas-phase O₂. From a mechanistic viewpoint, this reaction can run oxidatively or nonoxidatively with participation of lattice oxygen of oxidized VO_x species^[5-14] or their reduced counterparts,^[15,16] respectively. Although the former approach is thermodynamically not limited,

it suffers from low on-stream stability caused by a reduced capacity of VO_x species to provide their active oxygen. Recently, VO_x/SiO₂-Al₂O₃ catalysts were shown to have commercially attractive activity, propylene selectivity and durability in propane DH.^[15,16] The latter is an important process parameter, because all known DH catalysts suffer from deactivation caused by coke deposits formed on their surface.^[17,18] To remove coke and restore the initial activity and selectivity, catalysts must be oxidatively regenerated. Such regeneration results in restructuring of the active Pt and CrO_x species and, consequently, in a gradual loss of the catalytic performance with a growing number of DH/regeneration cycles,^[19] while VO_x-based catalysts remain stable.^[15,16] It was also demonstrated that VO_x/MCM-41 maintains higher stability than its CrO_x counterpart in a given DH cycle,^[15] which, combined with VO_x better durability, sets a case for further investigation of vanadium oxide catalysts as a potential alternative to commercial chromium oxide analogs.

Thorough understanding of the process(es) responsible for coke deposition and removal is highly important for further development of novel or improving of the existing catalysts. The analytical methods typically employed to study the phenomenon include temperature-programmed oxidation of spent catalysts, as well as in situ spectroscopic and thermogravimetric techniques. The latter in situ methods allow kinetic analysis of coke formation and thus make deeper fundamental understanding of coke formation possible. They were instrumental in elucidating relations between coking behavior and catalytic activity in several reactions^[20-23] including propane dehydrogenation on CrO_x^[24,25] and Pt-based^[26-28] catalysts. To our knowledge, there are no mechanistic and kinetic studies of coke formation in propane DH over VO_x-based catalysts.

[a] Dr. S. Sokolov, Dr. M. Stoyanova, Dr. U. Rodemerck, Dr. U. Bentrup, Dr. D. Linke, Dr. E. V. Kondratenko
Leibniz-Institut für Katalyse e.V. an der Universität Rostock
Albert-Einstein-Str. 29 a,D-18059 Rostock (Germany)
E-mail: Evgenii.Kondratenko@catalysis.de

[b] Dr. V. Y. Bychkov, Dr. Y. P. Tyulenin, Prof. V. N. Korchak
Semenov Institute of Chemical Physics
Russian Academy of Sciences
Kosygina str. 4, GSP-1, Moscow 119991 (Russia)

Supporting Information for this article is available on the WWW under <http://dx.doi.org/10.1002/cctc.201500151>.

The purpose of the current work was to elucidate physico-chemical properties of VO_x-based catalysts responsible for coke deposition in propane DH and hence detrimental for their on-stream stability. To this end, we prepared catalysts comprising highly dispersed or polymerized VO_x species on the supports of different acidity [SiO₂, Al₂O₃, and SiO₂-Al₂O₃ (Siral)] as well as nanocrystalline V₂O₅ on a single selected Siral. Their on-stream activity and selectivity in propane DH were determined under industrially relevant conditions, and the kinetics of coke formation was derived from time-resolved in situ thermogravimetric experiments.

Results and Discussion

Determination of VO_x molecular structures

The degree of polymerization of surface VO_x species was evaluated by in situ UV/Vis spectroscopy at 550 °C in air to exclude the effect of adsorbed water. This technique has been successfully employed by many researchers to distinguish between isolated, polymerized VO_x species or crystalline V₂O₅ in supported vanadium-containing catalysts.^[29–40] In Figure 1, the UV/Vis spectra of 5V/MCM-41, 4V/S10, 6V/S10, 13V/S10 and 3V/Al₂O₃ are shown (for abbreviations see Experimental Section). Briefly, the number in front gives the rounded vanadium weight content, the index in the Siral formula stands for a weight percentage of SiO₂. The spectra of other V/Siral catalysts with V loading of 4–5 wt% were similar to that of 4V/S10.

A broad adsorption maximum at approximately 300 nm in the spectrum of 5V/MCM-41 stems from O²⁻ to V⁵⁺ charge-transfer transitions and is characteristic of highly dispersed dehydrated VO₄ species.^[33,36,37,41] The red shift and broadening of the maximum take place if such species become connected via oxygen bridges or if three-dimensional V₂O₅ is formed.^[33,37,41] For a qualitative comparison of the catalysts with respect to the kind of VO_x species, we calculated the edge energy (E_{Edge}) from the UV/Vis spectra according to the procedure described in Ref. [42]. The results are given in Table 1. As expected, E_{Edge} decreased with increasing apparent V surface density (Figure 2a) and reached the lowest value for 13V/S10. This catalyst possessed crystalline V₂O₅ [PDF#00-074-1595] with an average crystallite size of 65 nm as determined by XRD analysis, whereas all other samples were free of XRD-detectable vanadia.

However, the loading and hence the surface V density was not the only factor determining the degree of polymerization of VO_x species. Acidity of the supports on which VO(acac)₂ was grafted also influenced the final distribution of VO_x species, as shown in Figure 2b. Clearly, for the catalysts with low V surface coverage, E_{Edge} decreases with an increase in acidity of the corresponding pristine supports. In other words, higher acidity

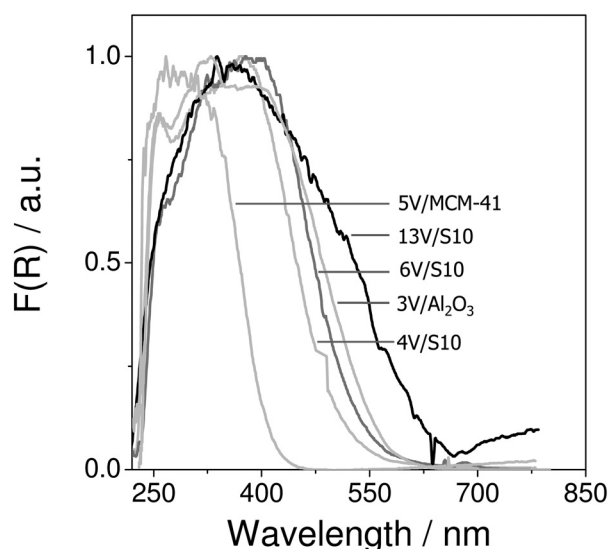


Figure 1. UV/Vis spectra of selected catalysts collected at 550 °C in air.

favors formation of higher polymerized VO_x species. Contrarily, for the catalysts with high V surface density, for example, 13V/S10 and, to a lesser extent, 6V/S10, VO_x particles were larger than follows from the trend. This deviation suggests that support acidity plays less or no role in determining the size of VO_x particles if the support surface coverage with V approaches or exceeds a monolayer.

On-stream catalytic performance

For all catalysts tested, propylene was the main product, and methane, ethane, ethylene, and C₄ and C₅ hydrocarbons were gas-phase side products. In Figure 3 propane conversion is shown as a function of time on stream. The corresponding data for selectivity to propylene and carbon are given in Supporting Information, Figure S1. For all catalysts, the initial propane conversion was below the equilibrium conversion of 0.43 calculated for the current experimental conditions. Clearly, the catalysts differed substantially in their on-stream stability and selectivity to carbon. 5V/MCM-41 and 5V/S70 showed the highest stability and the lowest carbon selectivity with the latter being between 1 and 5% over the duration of DH test. In contrast, this selectivity over other tested catalysts dropped

Table 1. Physico-chemical properties of catalysts and rate constants of deactivation (k_{deac}) and carbon deposition over the catalyst surface ($k_{\text{coke}(m)}$) and over already existing carbon layer ($k_{\text{coke}(M)}$).

Catalyst	V [wt. %]	$S_{\text{BET}}^{[a]}$ [m ² g ⁻¹]	E_{Edge} [eV]	k_{DH} [mol kg ⁻¹ Pa ⁻¹ s ⁻¹]	k_{deac} [min ⁻¹]	$k_{\text{coke}(m)}$ [min ⁻¹]	$k_{\text{coke}(M)}$ [min ⁻¹]
3V/Al ₂ O ₃	2.7	74 (89)	1.87	3.8×10^{-8}	17.8×10^{-4}	5.5×10^{-3}	1.5×10^{-4}
4V/S1	4.3	235 (255)	2.08	6.1×10^{-8}	11.3×10^{-4}	0.9×10^{-3}	0
4V/S10	4.2	280 (350)	2.11	6.3×10^{-8}	10.5×10^{-4}	1.1×10^{-3}	0
6V/S10	6.4	276 (350)	1.98	6.8×10^{-8}	14.0×10^{-4}	1.8×10^{-3}	0
13V/S10	13.2	150 (350)	1.72	4.0×10^{-8}	18.3×10^{-4}	7.1×10^{-3}	2.1×10^{-4}
5V/S40	5.1	353 (475)	2.13	5.4×10^{-8}	10.0×10^{-4}	0.6×10^{-3}	0
5V/S70	4.6	266 (360)	2.24	2.4×10^{-8}	4.3×10^{-4}	0.5×10^{-3}	0
5V/MCM41	4.9	810 (901)	2.76	4.4×10^{-8}	3.9×10^{-4}	0.5×10^{-3}	0

[a] BET surface area of pristine supports is given in parentheses.

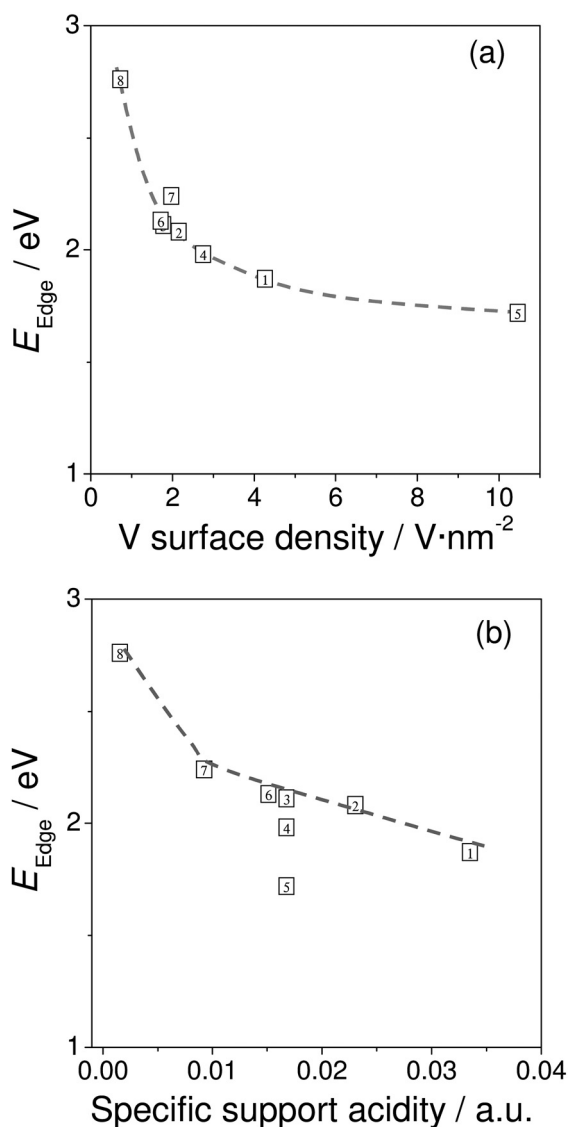


Figure 2. E_{Edge} of VO_x species versus a) apparent V surface density and b) specific support acidity measured by in situ FTIR pyridine adsorption at 150°C : Numbers in the squares: 1) $3\text{V}/\text{Al}_2\text{O}_3$, 2) $4\text{V}/\text{S1}$, 3) $4\text{V}/\text{S10}$, 4) $6\text{V}/\text{S10}$, 5) $13\text{V}/\text{S10}$, 6) $5\text{V}/\text{S40}$, 7) $5\text{V}/\text{S70}$, and 8) $5\text{V}/\text{MCM-41}$. Apparent V surface density was calculated as a ratio of V atoms to catalyst surface area.

from approximately 15% at the beginning to zero towards the end of the test. The decrease in S_{carbon} was concomitant with the activity loss, which was especially rapid on $3\text{V}/\text{Al}_2\text{O}_3$ and $13\text{V}/\text{S10}$, making these two catalysts the least stable.

To quantitatively compare the catalysts in terms of their on-stream stability, we estimated the constant of deactivation rate by fitting of the experimental data in Figure 3 to the kinetic model expressed in Equation (1). The deactivation rate was assumed to be of the first order and independent of the concentration of gas-phase species. The reactor was modeled as isothermal plug-flow. Both the constant of deactivation rate (k_{deac}) and the constant of propane dehydrogenation (k_{DH}) were the fitting parameters.

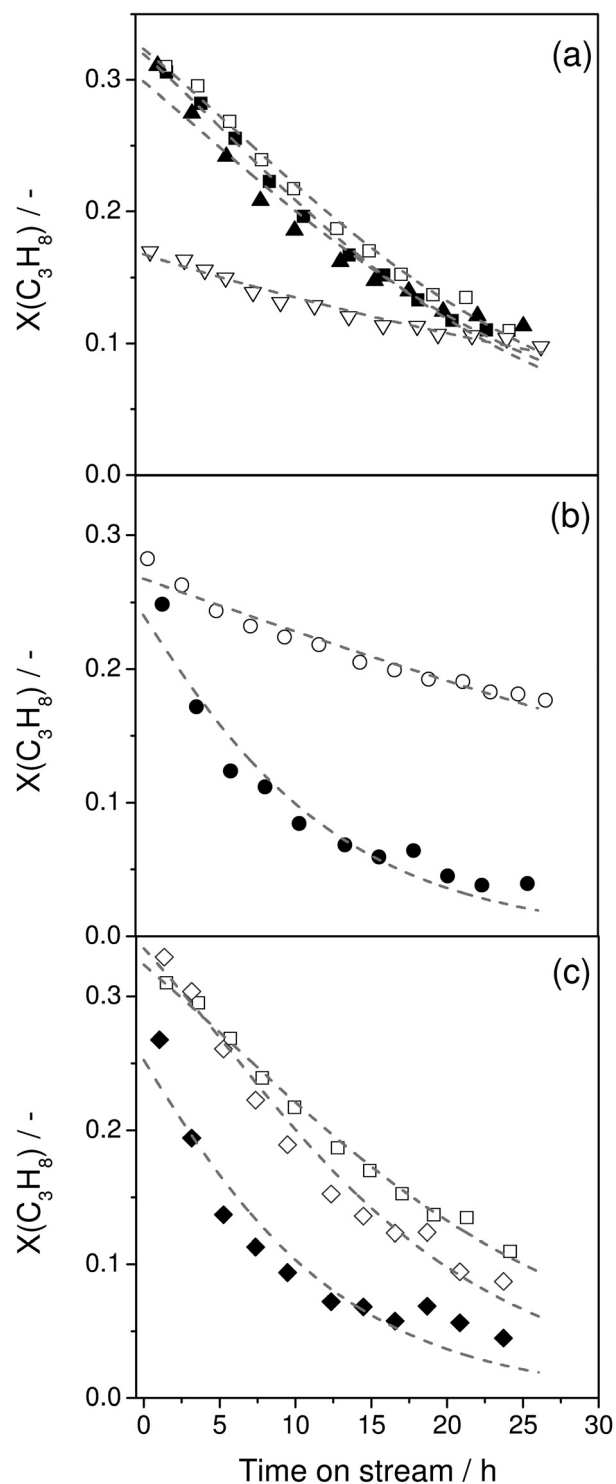


Figure 3. On-stream propane conversion over a) V/Sirals with V loading 4–5 wt.%; b) $5\text{V}/\text{MCM-41}$ and $3\text{V}/\text{Al}_2\text{O}_3$; and c) V/S10 with V loading of 4.2, 6.4, and 13.2 wt.%. Test conditions: 550°C , $\text{C}_3\text{H}_8/\text{N}_2 = 40:60$, $\text{WHSV} = 0.94 \text{ h}^{-1}$. Dashed lines were calculated by using Equation (1). \bullet , $3\text{V}/\text{Al}_2\text{O}_3$; \blacksquare , $4\text{V}/\text{S1}$; \square , $4\text{V}/\text{S10}$; \diamond , $6\text{V}/\text{S10}$; \blacklozenge , $13\text{V}/\text{S10}$; \blacktriangle , $5\text{V}/\text{S40}$; \blacktriangledown , $5\text{V}/\text{S70}$; and \circ , $5\text{V}/\text{MCM-41}$.

$$r = \exp(-k_{\text{deac}} \times t) \times [k_{\text{DH}} \times p(\text{C}_3\text{H}_8) - k_{\text{DH}}/K_{\text{eq}} \times p(\text{H}_2) \times p(\text{C}_3\text{H}_6)] \quad (1)$$

where $p(\text{C}_3\text{H}_8)$, $p(\text{C}_3\text{H}_6)$, and $p(\text{H}_2)$ are the partial pressures of the respective gases. K_{eq} is the equilibrium constant of propane DH (1.36×10^4 Pa at 550°C) and t is time.

In Figure 3, the experimental data points and the “deactivation” curves obtained through modeling are displayed. Apparently, the model correctly predicts evolution of propane conversion with time on stream over all catalysts. The deactivation rate constant (k_{deac}) obtained from the fitting is given in Table 1.

If k_{deac} values are related to the corresponding E_{Edge} (Table 1, Figure 6d), it becomes evident that k_{deac} increases as E_{Edge} decreases, that is, smaller VO_x species (high E_{Edge}) deactivate slower. To gain further fundamental insight into this relationship, we analyzed the kinetics of carbon formation under propane DH conditions by means of thermogravimetric analysis (TGA) with a simultaneous analysis of gas-phase products.

In situ monitoring of catalyst reduction and carbon deposition

In Figure 4, the weight-change curves are shown obtained in the in situ TGA experiments on the catalysts in a flow of $\text{C}_3\text{H}_8/\text{He} = 50:50$. For all catalysts, the curves feature an initial drop followed by a rise, yet their temporal evolution strongly varies between the catalysts. The initial weight loss commences in two steps occurring in the temperature ranges of $90\text{--}450$ and $450\text{--}550^\circ\text{C}$ (Figure S2). The mass spectrometry (MS) measurements performed simultaneously with TGA revealed evolution of water on all catalysts also proceeding in two steps with the maxima falling into the $170\text{--}270^\circ\text{C}$ and $500\text{--}550^\circ\text{C}$ ranges (Figure S3).

The first step was ascribed to desorption of physically adsorbed water, and the second to the loss of lattice oxygen from VO_x species upon their reduction by propane and/or reaction products. The latter phenomenon was reported in several previous studies.^[43–49] Dehydroxylation of the surface may occur in a wider range of temperatures and thus contributes to both weight-loss steps. Noteworthy is the difference between 13V/S10 and two other V/S10 catalysts (Figure S3c). On the former, the low-temperature peak of water desorption (at $\approx 190^\circ\text{C}$) is negligible compared to the one related to water formation through reduction of VO_x species by propane in the $300\text{--}550^\circ\text{C}$ range. On the latter two catalysts, both peaks are of comparable height. Recalling that Siral10 surface in 13V/S10 is covered by more than a monolayer of VO_x , it can be hypothesized that water adsorption on VO_x and V_2O_5 is hindered compared to that on Siral10 resulting in a relatively small “desorption” peak. On other hand, the “reduction” peak of 13V/S10 has two maxima caused by participation of surface and bulk lattice oxygen of V_2O_5 in water formation.

Besides H_2O , H_2 was observed during the second step of weight loss indicating beginning of nonoxidative DH reaction. Simultaneous evolution of water and hydrogen stems from the fact that oxidative and nonoxidative dehydrogenation run concurrently at the earliest stage of the reaction over initially oxidized catalysts. After approximately 20 min on stream, the intensity of H_2O signal drops sharply suggesting that VO_x reduc-

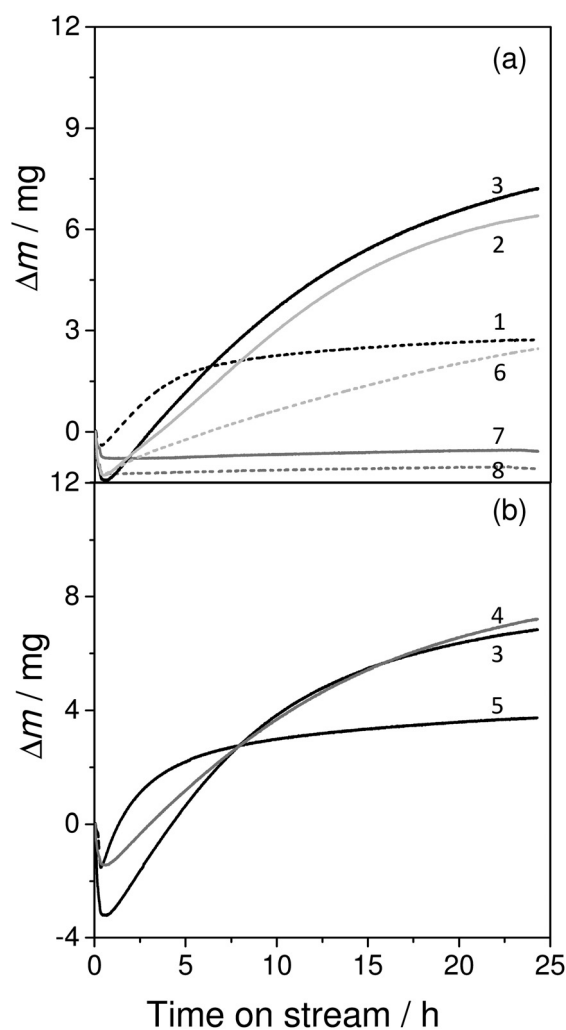


Figure 4. TGA profiles recorded during propane DH over the catalysts with a) V loading of 3–5 wt.% and b) over V/S10 with V loading of 4.2, 6.4, and 13.2 wt.%. Test conditions: 550°C , $\text{C}_3\text{H}_8/\text{He} = 50:50$. Catalyst numbers are defined in Figure 2.

tion likewise oxidative propane dehydrogenation are largely completed. The intensity of H_2 keeps growing indicating that the DH reaction proceeds further via a nonoxidative route.

Once water is removed from the catalysts through the processes discussed above, the weight curves start ascending because of continuous accumulation of coke on the catalysts. It is evident that the trends in weight increase in Figure 4 varied dramatically between the catalysts. 4V/S1 and 4V/S10 showed the strongest weight gain that lasted over entire duration of the experiment. Contrarily, the weight curves of 3V/ Al_2O_3 and 13V/S10 are characterized by fast increase in the first 6 h on stream followed by a moderate growth phase that flattened into a plateau by the end of the experiment. Specifically, during the first 6 h on stream, 3V/ Al_2O_3 and 13V/S10 added respectively 73 and 65% of their total weight gain. Further, 5V/S40 sustained a slow increase through the whole test, whereas 5V/S70 and 5V/MCM-41 gained very little weight.

To compare the rates of carbon deposition on different catalysts quantitatively, we kinetically evaluated the weight change

curves starting from the second step of water formation (oxidative dehydrogenation of propane). To this end, we used Equation (2) for describing both oxygen removal from VO_x and coke deposition (descending and ascending parts of the TGA curves in Figure 4 respectively). The first term in this equation accounts for coke formation as originally suggested in Refs.^[24–26] for evaluation of similar experiments of propane dehydrogenation over Pt- and CrO_x -based catalysts. In these studies, coke formation with its own kinetics was assumed to take place i) over coke-free surface of the catalysts to yield “carbon” monolayer as well as ii) over formed coke species resulting in multilayer deposits. The second term in Equation (2) describes removal of lattice oxygen from oxidized (+5 or +4) VO_x species in form of water and carbon oxides.

$$\Delta m = \Delta m_{\text{coke}} \times (1 - \exp(-k_{\text{coke}}(m) \times t) + k_{\text{coke}}(M) \times t) - \Delta m_{\text{O}} \times (1 - \exp(-k_{\text{O}} \times t)) \quad (2)$$

where Δm_{coke} is a weight gain from a monolayer of carbon, $k_{\text{coke}}(m)$ and $k_{\text{coke}}(M)$ respectively are the rate constants of coke formation over carbon-free catalyst surface and over already existing carbon deposits. Δm_{O} and k_{O} stand for a weight loss upon reduction of oxidized VO_x species and the rate constant of this process.

The kinetic model assumed here provides a good description of the weight curves. The experimental TGA data and their fitting are shown in Figure 5 for 5V/MCM-41 and 4V/S10 selected as examples of the catalysts with very different coking behavior. The data fitting overlays for other catalysts are given in Figure S4. Importantly, the goodness of fit of the curves for all catalysts with the exception of 3V/ Al_2O_3 and 13V/S10 was not sensitive to the $k_{\text{coke}}(M)$ value. The latter therefore could be set to zero suggesting that not enough carbon was deposited to form a monolayer. In the case of 3V/ Al_2O_3 and 13V/S10, inclusion of $k_{\text{coke}}(M)$ in the fitting procedure improved the goodness of fit significantly indicating that carbon monolayer was formed on these two catalysts and further coke deposition took place over that monolayer. Apparently, one reason behind formation of the monolayer on 3V/ Al_2O_3 and 13V/S10 is their low specific surface area.

As seen from Table 1, the obtained values of $k_{\text{coke}}(M)$ are in general significantly lower than those of $k_{\text{coke}}(m)$ meaning that formation of coke on already deposited carbon layer proceeds much slower than on carbon-free surfaces of the catalysts. It is in agreement with the results previously obtained for coke formation in propane DH over $\text{Cr}_2\text{O}_3/\text{Al}_2\text{O}_3$ described by the same kinetic model.^[25] Two important observations regarding the rate constant of coke formation over carbon-free surfaces should be emphasized:

For the catalysts with V loading of 3–5 wt%, $k_{\text{coke}}(m)$ increases with Al content in the support from the minimum on 5V/MCM-41 ($0.5 \times 10^{-3} \text{ min}^{-1}$) to the maximum on 3V/ Al_2O_3 ($5.49 \times 10^{-3} \text{ min}^{-1}$).

Vanadium loading and consequently its surface density also influence the $k_{\text{coke}}(m)$ constant. It rises from 1.96×10^{-3} to

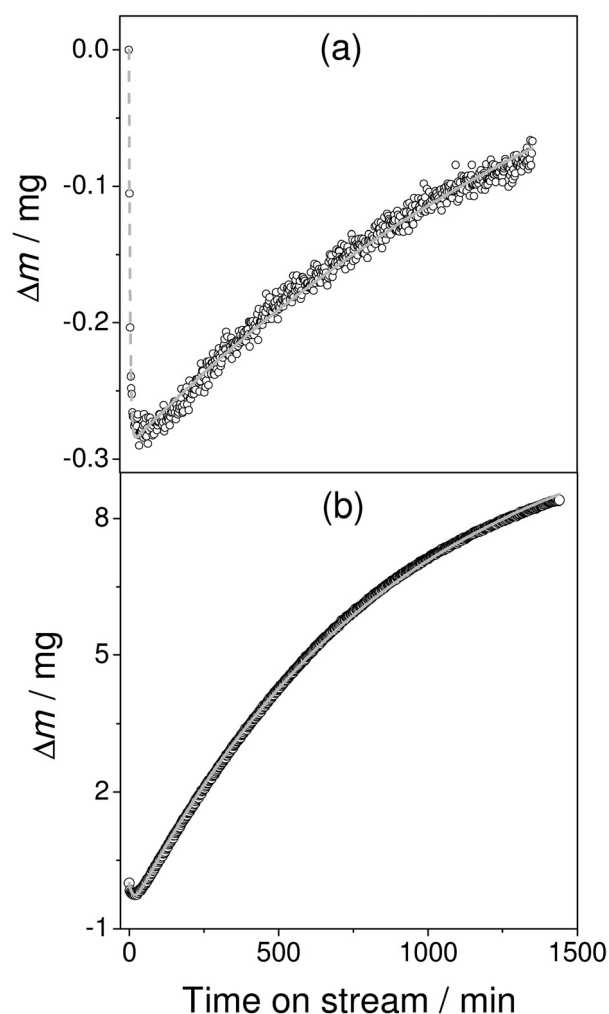


Figure 5. Comparison between calculated (line) and experimental (open circles) TGA profiles recorded during propane DH over a) 5V/MCM-41 and b) 4V/S10. Experimental conditions as in Figure 4.

$7.07 \cdot 10^{-3} \text{ min}^{-1}$ as V loading increases from 4.2 to 13.2 wt% for the V/S10 catalysts.

Factors governing coke formation and on-stream stability

Catalyst acidity is often reported to be one of the important parameters determining coke formation and deactivation in nonoxidative dehydrogenation of C_2 – C_4 alkanes.^[50–55] To test this hypothesis, we constructed plots showing the relationship between surface-normalized catalyst acidity and the rate constants of coke formation $k_{\text{coke}}(m)$ (Figure 6a) and catalyst deactivation k_{deac} (Figure 6b). Despite the fact that most acidic 3V/ Al_2O_3 and 13V/S10 deactivated faster than all other catalysts, no general correlation for all tested catalysts could be discerned. Yet, if $k_{\text{coke}}(m)$ and k_{deac} are plotted versus E_{Edge} of VO_x species, one can see trends holding for all catalysts (Figure 6c and d). Both constants increase as E_{Edge} decreases suggesting that the degree of oligomerization of surface VO_x species affects coke formation and catalyst deactivation, that is, the

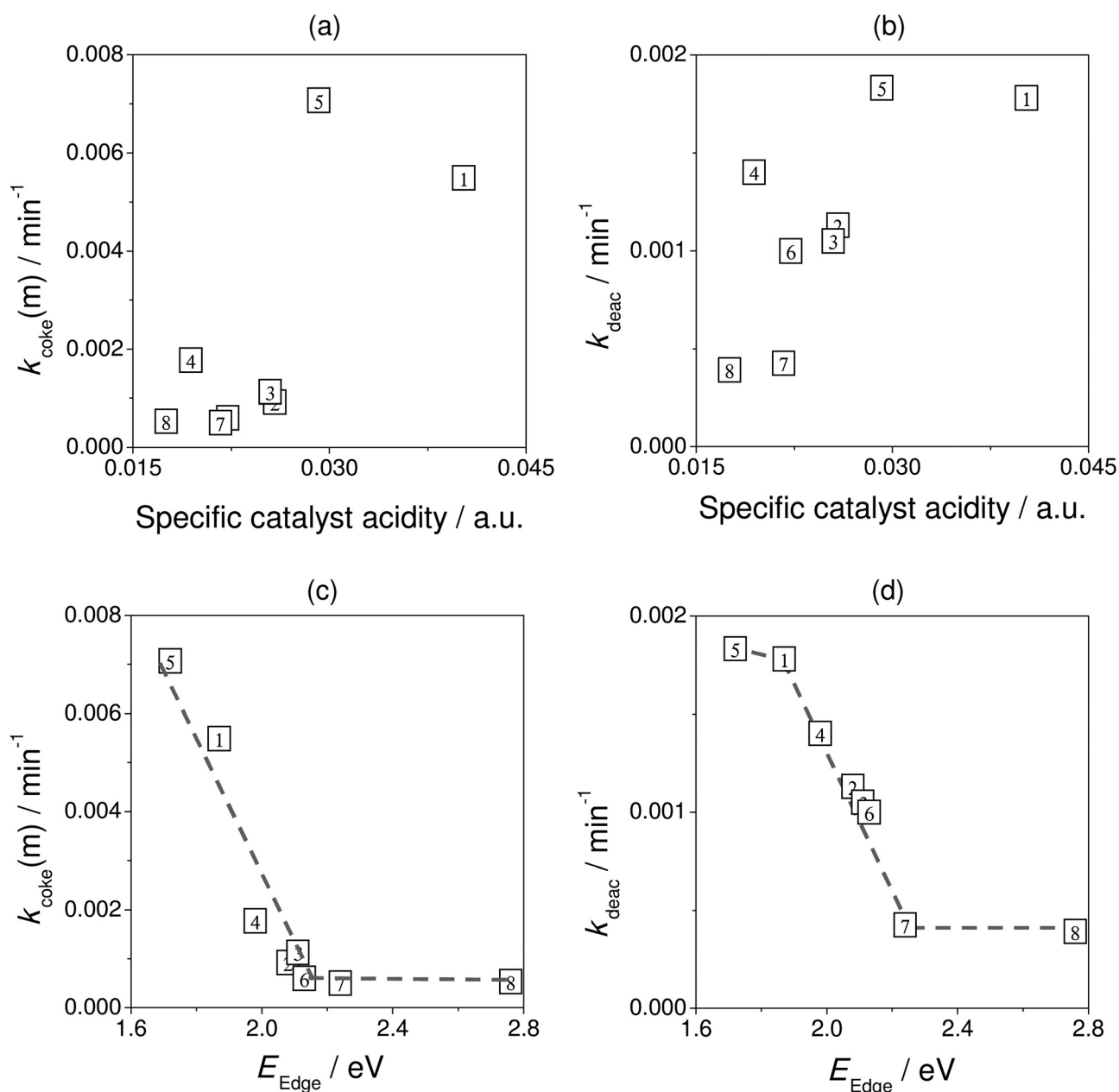


Figure 6. Rate constants of a, c) coke formation ($k_{\text{coke}}(\text{m})$) and b, d) catalyst deactivation (k_{deac}) versus a, b) surface-normalized catalyst acidity and c, d) edge energy of VO_x species. Catalyst numbers are defined in Figure 2.

larger the species, the faster these processes. Remarkably, loss of activity accelerates as carbon deposition mounts, which becomes especially visible if k_{deac} is plotted versus $k_{\text{coke}}(\text{m})$ as in Figure 7. This correlation suggests that carbon deposits directly on the surface of VO_x sites shielding them from propane and thus resulting in catalyst deactivation.

To deepen our understanding of the effect of VO_x species size on coke formation, we performed catalytic tests with a feed containing propylene (11.4 vol.% C_3H_6 in N_2) as it is known to be a coke precursor. To distinguish between the coke formed on the supports and on VO_x , the catalysts with highly dispersed, moderately, and highly polymerized VO_x species, that is, 5V/MCM-41, 4V/S10 and 3V/ Al_2O_3 , corresponding-

ly, and the respective pristine supports were investigated. After exposing the above catalysts and supports to the $\text{C}_3\text{H}_6/\text{N}_2$ feed for 3 h, the spent materials were analyzed by TPO to determine the amount of carbon deposits. The amount of deposited carbon is found in Table 2.

Zero propylene conversion was observed over pristine MCM-41, which remained snow-white after 3 h on stream. TPO analysis did not reveal any carbon-containing species on this material. Contrarily, propylene conversion and carbon deposits were observed on 5V/MCM-41. Therefore, we can safely conclude that coke formation on 5V/MCM-41 during the catalytic tests with propylene and propane occurred exclusively on VO_x species. In the case of 4V/S10, coke was formed on both the sup-

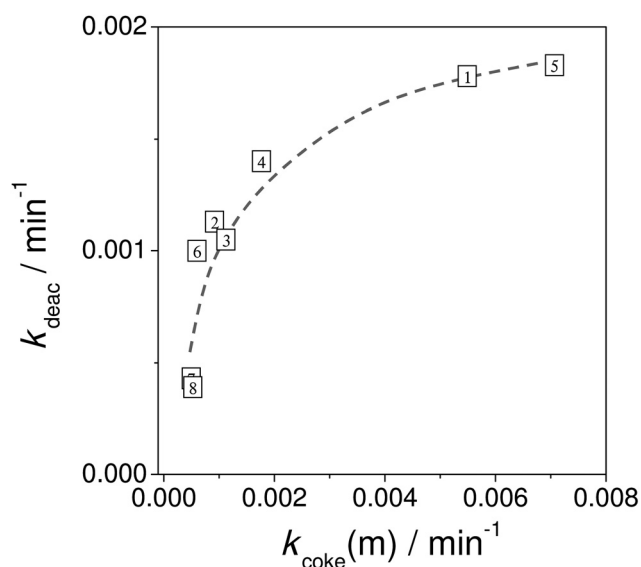


Figure 7. Catalyst deactivation constant k_{deac} versus rate constant k_{coke} of coke formation. Catalyst numbers are defined in Figure 2.

Catalyst	$m(\text{carbon})$ [mg g^{-1}]		$r_v(\text{carbon})$ per weight V [$\text{mg}(\text{C})\text{g}(\text{V})^{-1}\text{min}^{-1}$]
	Pure support	Catalyst	
3V/ Al_2O_3	8.4	74.0	1150
4V/S10	43.7	199.3	800
5V/MCM-41	0	128.2	650

port and VO_x . However, the amount deposited on 4V/S10 was 4.2 times higher than that on pristine S10. This evidences that VO_x species on this catalyst are significantly more active in coke formation than the support, especially given that the support is partially covered by VO_x . In the case of 3V/ Al_2O_3 , for which V coverage exceeds one monolayer, coke formation occurs entirely on VO_x ; the amount of carbon on the catalyst was 8.8 times higher than on pristine Al_2O_3 . These comparisons certainly verify that VO_x species function as the sites for coke formation and are substantially more active in this process than acidic sites on S10 and $\gamma\text{-Al}_2\text{O}_3$. The fact that the amount of carbon deposited on 3V/ Al_2O_3 and Al_2O_3 is lower than on other catalysts and pristine S10 stems from their fast deactivation.

Returning to the correlation between size and activity of VO_x species in coke formation, we calculated the initial rate (r_v) of carbon formation per weight of V [Eq. (9)] for estimating intrinsic activity of differently sized VO_x species. The activity of acidic sites on S10 was neglected for the reasons discussed above. The rate values found in Table 2 indicate that carbon deposition on 3V/ Al_2O_3 proceeds much faster than on 5V/MCM-41. Recalling that a certain fraction of V atoms on the former catalyst is buried in multilayers, the difference between the catalysts must be even larger. The r_v obtained on 4V/S10 falls be-

tween the values of 3V/ Al_2O_3 and 5V/MCM-41, which matches the arrangement of the catalysts' VO_x species according to their size.

Based on the fact that coke deposition takes place on VO_x species, the effect of their size on coking rate can be explained as follows. From a mechanistic viewpoint, adsorbed propylene molecules interact with each other to initially form small aromatic structure followed by further oligomerization and condensation to large graphitic structures.^[9] As for isolated VO_x sites, they should be located in close proximity to each other to oligomerize. Alternatively, adsorbed propylene or its fragments may migrate from one VO_x species to another, on which they can further transform into coke. Upon increasing apparent V surface density and the size of VO_x species, a probability of interaction between several adsorbed propylene molecules increases resulting in a higher rate of carbon deposition. The highest rate will be achieved if the support surface is completely covered by highly polymerized VO_x species or crystalline V_2O_5 as in 3V/ Al_2O_3 . Exactly this trend was observed experimentally.

Conclusions

Nonoxidative propane dehydrogenation to propylene over VO_x species supported on $\text{Al}_2\text{O}_3\text{-SiO}_2$ with SiO_2 content varying from 0 to 100 wt.% was studied in conventional catalytic tests and by in situ thermogravimetric analysis (TGA). Kinetic evaluation of the obtained data combined with characterization of VO_x species allowed novel insight into coke formation. Irrespective of the kind of the supported VO_x species, they are more active in coke formation from propylene than acidic sites of the supports. The kinetic analysis of TGA profiles enabled us to conclude that carbon monolayer-multilayer model quite accurately described this process. A clear correlation between the rate constant of carbon deposition and that of catalyst deactivation was found thus verifying that resistance to coking determines catalysts on-stream stability. Importantly, the rate constant of carbon deposition strongly increased with the degree of VO_x polymerization reaching the maximum on nanocrystalline V_2O_5 . This tendency was rationalized through a general mechanism of coke formation. To form carbon precursors from adsorbed propylene or its fragments, they should be located in close proximity to each other. Such situation is easily realized on large VO_x species, whereas on the smaller ones it is statistically less probable. As coke formation proceeds faster on larger VO_x particles, the catalysts designed for long-term stability in propane dehydrogenation shall have high coverage of the support with small or even isolated VO_x species.

Experimental Section

Preparation of catalytic materials

To prepare supported catalysts we used $\gamma\text{-Al}_2\text{O}_3$ (NorPro Saint-Gobain), SiO_2 (MCM-41) and $\text{SiO}_2\text{-Al}_2\text{O}_3$ (Siral 1, 10, 40, and 70, provided by Sasol) as supports. The index in the Siral formula stands for a weight percentage of SiO_2 . MCM-41 was synthesized as described in Ref. [56]. The support densities starting from Al_2O_3 and

going in the direction of increasing SiO₂ content were 0.641, 0.591, 0.517, 0.352, 0.313, and finally 0.303 g cm⁻³ for MCM-41. The procedure from Ref. [16] was used for deposition of VO_x species on the supports. Briefly, vanadyl acetylacetonate (VO(acac)₂, 2.6 g) was dissolved in dry toluene (1 L). Hereafter, a dried support (10 g) was added to this solution, which was then stirred for 24 h. Then the solid was isolated, washed in toluene twice, dried, and calcined in air at 550 °C for 12 h. To deposit higher loadings of VO_x on Siral 10, we used amounts of VO(acac)₂ of 9.4 or 18.8 g to prepare 1 L toluene solutions. The catalysts are abbreviated as 3V/Al₂O₃, 4V/S1, 4V/S10, 6V/S10, 13V/S10, 5V/S40, 5V/S70, and 5V/MCM-41 with vanadium weight content rounded to the whole number shown in front of the abbreviation. The exact content is given in Table 1.

Catalyst characterization

Nitrogen adsorption isotherms collected at 77 K on BELSORP-mini II (BEL Japan) were used to calculate the specific surface area of the calcined catalysts applying the Brunauer, Emmet and Teller (BET) equation for N₂ relative pressure range of 0.05 < P/P₀ < 0.30. The BET values are provided in Table 1.

The vanadium content of the calcined catalysts was determined by inductively coupled plasma optical emission spectroscopy (ICP-OES, Varian 715-ES).

X-ray diffraction was performed on the theta/theta diffractometer X'PertPro from Panalytical (Almelo; The Netherlands) equipped with the X'celerator RTMS detector system using Cu Kα 1/2 radiation (λ = 1.5418 Å, 40 kV, 40 mA). The alignment was checked against a silicon standard. The data were collected in the 2θ range of 5–70° with a total measurement time of 12 min. The phase composition of the samples was determined using the program suite WINXPow by STOE&CIE with inclusion of the Powder Diffraction File PDF2 of the ICDD (International Centre of Diffraction Data). The Scherrer equation was applied to calculate the V₂O₅ [PDF#00-074-1595] average crystallite size from the reflection at 2θ of 26.13°.

The UV/Vis spectra of fresh catalysts were collected at 550 °C using an in-house developed setup described in Ref. [57]. Prior to the analysis, the samples were conditioned at the same temperature in a flow of synthetic air for 1 h. The AVASPEC UV/Vis spectrometer (Avantes) used in the study was equipped with a DH-2000 deuterium-halogen light source and a CCD array detector. BaSO₄ was used as a white reference standard. All UV/Vis spectra are presented as Kubelka-Munk function $F(R_{\infty})$ calculated according to Equation (3),

$$F(R_{\infty}) = \frac{(1 - R_{\infty})^2}{2 \times R_{\infty}} \quad (3)$$

where R_{∞} is reflection.

For determining catalyst acidity, we performed IR measurements of adsorbed pyridine. They were performed in transmission mode on a Bruker Tensor 27 FT IR spectrometer equipped with a heated and evacuated custom made reaction cell with CaF₂ windows connected to a gas dosing and evacuation system. The powdery samples (50 mg) were pressed into self-supporting wafers with a diameter of 20 mm. Before pyridine adsorption, the samples were pretreated at 400 °C for 10 min in synthetic air followed by cooling to 150 °C and evacuation. Pyridine was adsorbed at 150 °C until saturation. Then the reaction cell was evacuated for removing physisorbed

pyridine. The IR spectra of adsorbed pyridine were recorded at 150 °C.

Continuous-flow catalytic tests

Catalytic propane DH tests were performed in a multichannel setup equipped with 15 plug-flow fixed-bed quartz tube reactors (Ø_{id} = 3.8 mm) operated in parallel. Each reactor was filled with 300 mg (315–710 μm grain fraction) of the fresh catalyst. The catalysts were heated to 550 °C (5 K min⁻¹) in synthetic air (10 mL min⁻¹ per reactor), held in the air flow for 1 h and then purged with N₂ for 20 min. Hereafter a mixture of 40 vol% C₃H₈ in N₂ was fed at a rate of 6 mL min⁻¹ per reactor. All catalytic experiments were performed at a weight hourly space velocity (WHSV) of 0.94 h⁻¹ and a pressure of 1.2 bar. The experiments were run for 25 h followed by cooling the reactors to RT in N₂. Catalytic experiments aimed to study coking behavior of selected catalysts and their respective supports were performed in a feed containing 11.5 vol% of propylene in nitrogen at 550 °C. This propylene concentration was determined to be an average in propane DH tests. The experiments designed to quantify the amount of carbon deposited on catalysts and supports were performed at WHSV of 0.26 h⁻¹ and lasted for 3 h. To find the initial propylene conversion rates, 5V/MCM-41, 4V/S10 and 3V/Al₂O₃ were tested at WHSV of 2.6 h⁻¹ for 1 h. The initial rates of propylene conversion were calculated as mol(C₃H₆) converted per mol(V) per hour at zero time on stream. The initial conversion values were obtained from fitting the X(C₃H₆) curves by Equation (1).

The feed components and the reaction products were analyzed by an on-line gas chromatograph (Agilent 6890N) equipped with PLOT/Q (for CO₂), HP-PLOT Al₂O₃ "KCl" (for hydrocarbons) and Mol-sieve5 (for H₂, O₂, N₂, and CO) columns, flame ionization and thermal conductivity detectors. The analyses were performed successively, reactor by reactor. The propane conversion $X(C_3H_8)$ was calculated from the inlet ($\dot{n}_{C_3H_8}^{inlet}$) and outlet ($\dot{n}_{C_3H_8}^{outlet}$) propane molar flows [Eq. (4)]. The outlet flow was corrected with respect to the flow of nitrogen to take into account reaction-induced changes in the number of moles of gas-phase components. The propylene yield $Y(C_3H_6)$ and selectivity to propylene $S(C_3H_6)$ and carbon $S(carbon)$ were calculated according to Equations (5), (6), and (7), respectively. Yield and selectivity of the side products methane, ethane, ethylene, C₄ and C₅ hydrocarbons, CO, and CO₂ were calculated accordingly taking into account their different numbers of C atoms.

$$X(C_3H_8) = \frac{\dot{n}_{C_3H_8}^{inlet} - \dot{n}_{C_3H_8}^{outlet}}{\dot{n}_{C_3H_8}^{inlet}} \quad (4)$$

$$Y(C_3H_6) = \frac{\dot{n}_{C_3H_6}^{outlet}}{\dot{n}_{C_3H_8}^{inlet}} \quad (5)$$

$$S(C_3H_6) = \frac{\dot{n}_{C_3H_6}^{outlet}}{\dot{n}_{C_3H_8}^{inlet} - \dot{n}_{C_3H_8}^{outlet}} \quad (6)$$

$$S(carbon) = \frac{X(C_3H_8) - \sum_i Y_i}{X(C_3H_8)} \quad (7)$$

$$Y(carbon) = X(C_3H_8) - \sum_i Y_i \quad (8)$$

$$r_v(carbon) = \frac{Y(carbon) \times \dot{m}(C_3H_6)}{m_v} \quad (9)$$

Where $\dot{n}_{C_3H_6}^{outlet}$, $\dot{m}(C_3H_6)$ and m_V are molar flow of propylene at the reactor outlet, weight flow of propylene at the reactor inlet, and weigh of vanadium in reactor respectively. Subscript i stands for any gas-phase products measured.

In situ thermogravimetric and temperature-programmed tests

The thermogravimetric setup described in Ref. [20] consisted of a thermobalance SETSYS Evolution (Setaram) and an on-line mass spectrometer OmniStar GSD 301 (Pfeiffer). A catalyst sample (50 mg) was loaded into a quartz cap suspended inside a thermobalance furnace. The sample was heated to 550 °C at 10 Kmin⁻¹ in a flow of 7.7% O₂ in He and held at this temperature for 12 h to oxidize VO_x species. After cooling to RT, a C₃H₈:He = 50:50 mixture was fed at 20 mL min⁻¹ for approximately 30 min. Hereafter, the reactor was heated to 550 °C at 30 Kmin⁻¹ in the same flow and held at this temperature for 24 h. Weight of the sample was continuously measured over the entire experiment. The reaction products and propane were monitored by mass spectrometry.

The amount of carbon deposits formed during catalytic experiments was determined from the amount of CO and CO₂ evolved during temperature-programmed oxidation (TPO) of spent catalysts. TPO measurements were performed in a setup equipped with eight individually heated plug-flow fixed-bed quartz tube reactors of 6.9 mm inner diameter. The used catalysts were heated to 900 °C at 10 Kmin⁻¹ in a flow (10 mLmin⁻¹) of 10 vol.% O₂ in Ar. Oxygen consumption and formation of reaction products were monitored by a quadrupole mass spectrometer (Pfeiffer Vacuum OmniStar 200). The following atomic mass units (AMUs) were analyzed: 44 (CO₂), 40 (Ar), 32 (O₂), 28 (CO, CO₂), and 18 (H₂O). The concentrations of O₂, CO, and CO₂ were determined from the respective AMUs using standard fragmentation patterns and sensitivity factors determined by analyzing calibration gas mixtures.

Acknowledgements

The authors are thankful to A. Simmula, M. Schneider, C. Rautenberg for assistance with sample characterization.

Keywords: carbon · dehydrogenation · kinetics · monolayers · vanadium

- W.-C. Cheng, E. T. Habib, Jr., K. Rajagopalan, T. G. Roberie, R. F. Wormsbecher, M. S. Ziebarth in *Handbook of Heterogeneous catalysis*, Vol. 6 (Eds.: G. Ertl, H. Knözinger, F. Schüth, J. Weitkamp), Wiley-VCH, Weinheim, **2008**, pp. 2741–2777.
- K. J. Caspary, H. Gehrke, M. Heinritz-Adrian, M. Schwefel in *Handbook of Heterogeneous Catalysis*, Vol. 7 (Eds.: G. Ertl, H. Knözinger, F. Schüth, J. Weitkamp), Wiley-VCH, Weinheim, **2008**, pp. 3206–3228.
- J. C. Mol, P. W. N. M. van Leeuwen in *Handbook of Heterogeneous Catalysis*, Vol. 7 (Eds.: G. Ertl, H. Knözinger, F. Schüth, J. Weitkamp), Wiley-VCH, Weinheim, **2008**, p. 3240.
- A. Aitani in *Encyclopedia of Chemical Processing*, Vol. 4 (Ed.: S. Lee), Taylor&Francis, New York, **2006**, p. 2461.
- M. E. Harlin, V. M. Niemi, A. O. I. Krause, *J. Catal.* **2000**, *195*, 67–78.
- M. E. Harlin, V. M. Niemi, A. O. I. Krause, B. M. Weckhuysen, *J. Catal.* **2001**, *203*, 242–252.
- H. Kwon, L. T. Thompson, J. Eng, Jr., J. G. Chen, *J. Catal.* **2000**, *190*, 60–68.
- S. D. Jackson, S. Rugmini, *J. Catal.* **2007**, *251*, 59–68.
- J. J. H. B. Sattler, J. Ruiz-Martinez, E. Santillan-Jimenez, B. M. Weckhuysen, *Chem. Rev.* **2014**, *114*, 10613–10653.
- J. McGregor, Z. Huang, G. Shiko, L. F. Gladden, R. S. Stein, M. J. Duer, Z. Wu, P. C. Stair, S. Rugmini, S. D. Jackson, *Catal. Today* **2009**, *142*, 143–151.
- Z. Wu, P. C. Stair, *J. Catal.* **2006**, *237*, 220–229.
- M. Volpe, G. Tonetto, H. de Lasa, *Appl. Catal. A* **2004**, *272*, 69–78.
- N. Ballarini, F. Cavani, M. Ferrari, R. Catani, U. Cornaro, *J. Catal.* **2003**, *213*, 95–102.
- N. Ballarini, F. Cavani, C. Cortelli, C. Giunchi, P. Nobili, F. Trifirò, R. Catani, U. Cornaro, *Catal. Today* **2003**, *78*, 353–364.
- S. Sokolov, M. Stoyanova, U. Rodemerck, D. Linke, E. V. Kondratenko, *J. Catal.* **2012**, *293*, 67–75.
- S. Sokolov, M. Stoyanova, U. Rodemerck, D. Linke, E. V. Kondratenko, *Catal. Sci. Technol.* **2014**, *4*, 1323–1332.
- E. Daniel, E. Resasco, G. L. Haller in *Catalysis*, Vol. 11 (Eds.: J. J. Spivey, S. K. Agarwal), Royal Society of Chemistry, Cambridge, **1994**, pp. 379–411.
- O. A. Bariäs, A. Holmen, E. A. Blekkan, *J. Catal.* **1996**, *158*, 1–12.
- A. Iglesias-Juez, A. M. Beale, K. Maaijen, T. C. Weng, P. Glatzel, B. M. Weckhuysen, *J. Catal.* **2010**, *276*, 268–279.
- V. Y. Bychkov, Y. P. Tyulenin, V. N. Korchak, E. L. Aptekar, *Appl. Catal. A* **2006**, *304*, 21–29.
- V. Y. Bychkov, Y. P. Tyulenin, A. A. Firsova, E. A. Shafranovsky, A. Y. Gorenberg, V. N. Korchak, *Appl. Catal. A* **2013**, *453*, 71–79.
- S. Chen, G. Manos, *J. Catal.* **2004**, *226*, 343–350.
- A. Platon, H.-S. Roh, D. King, Y. Wang, *Top. Catal.* **2007**, *46*, 374–379.
- J. A. Peña, A. Monzón, J. Santamaría, J. L. G. Fierro, *Appl. Catal. A* **1993**, *101*, 185–198.
- J. Gascón, C. Téllez, J. Herguido, M. Menéndez, *Appl. Catal. A* **2003**, *248*, 105–116.
- M. van Sint Annaland, J. A. M. Kuipers, W. P. M. van Swaaij, *Catal. Today* **2001**, *66*, 427–436.
- M. Santhosh Kumar, A. Holmen, D. Chen, *Microporous Mesoporous Mater.* **2009**, *126*, 152–158.
- M. Santhosh Kumar, D. Chen, A. Holmen, J. C. Walmsley, *Catal. Today* **2009**, *142*, 17–23.
- U. Scharf, M. Schraml-Marth, A. Wokaun, A. Baiker, *J. Chem. Soc. Faraday Trans.* **1991**, *87*, 3299–3307.
- F. Arena, F. Frusteri, G. Martra, S. Coluccia, A. Parmaliana, *J. Chem. Soc. Faraday Trans.* **1997**, *93*, 3849–3854.
- G. Catana, R. R. Rao, B. M. Weckhuysen, P. Van Der Voort, E. Vansant, R. A. Schoonheydt, *J. Phys. Chem. B* **1998**, *102*, 8005–8012.
- X. Gao, I. E. Wachs, *J. Phys. Chem. B* **2000**, *104*, 1261–1268.
- M. Baltes, K. Cassiers, P. Van Der Voort, B. M. Weckhuysen, R. A. Schoonheydt, E. F. Vansant, *J. Catal.* **2001**, *197*, 160–171.
- E. V. Kondratenko, M. Baerns, *Appl. Catal. A* **2001**, *222*, 133–143.
- N. Steinfeldt, D. Muller, H. Berndt, *Appl. Catal. A* **2004**, *272*, 201–213.
- E. V. Kondratenko, M. Cherian, M. Baerns, X. Su, R. Schlögl, X. Wang, I. E. Wachs, *J. Catal.* **2005**, *234*, 131–142.
- E. L. Lee, I. E. Wachs, *J. Phys. Chem. C* **2007**, *111*, 14410–14425.
- Z. Wu, H.-S. Kim, P. C. Stair, S. Rugmini, S. D. Jackson, *J. Phys. Chem. B* **2005**, *109*, 2793–2800.
- B. M. Weckhuysen, D. E. Keller, *Catal. Today* **2003**, *78*, 25–46.
- J. Słoczyński, R. Grabowski, A. Kozłowska, R. Tokarz-Sobieraj, M. Witko, *J. Mol. Catal. A* **2007**, *277*, 27–34.
- R. Bulánek, L. Čapek, M. Setnička, P. Čičmanec, *J. Phys. Chem. C* **2011**, *115*, 12430–12438.
- W. N. Delgass, G. L. Haller, R. Kellerman, J. H. Lunsford, *Spectroscopy in Heterogeneous Catalysis*, Academic Press, New York, **1979**.
- A. Pantazidis, S. A. Bucholz, H. W. Zanthoff, Y. Schuurman, C. Mirodatos, *Catal. Today* **1998**, *40*, 207–214.
- D. Creaser, B. Andersson, R. R. Hudgins, P. L. Silveston, *J. Catal.* **1999**, *182*, 264–269.
- K. Chen, E. Iglesia, A. T. Bell, *J. Catal.* **2000**, *192*, 197–203.
- K. Chen, A. T. Bell, E. Iglesia, *J. Catal.* **2002**, *209*, 35–42.
- R. Grabowski, J. Słoczyński, N. M. Grzesik, *Appl. Catal. A* **2002**, *232*, 277–288.
- N. Ballarini, F. Cavani, A. Cericola, C. Cortelli, M. Ferrari, F. Trifirò, G. Capannelli, A. Comite, R. Catani, U. Cornaro, *Catal. Today* **2004**, *91–92*, 99–104.
- E. V. Kondratenko, N. Steinfeldt, M. Baerns, *Phys. Chem. Chem. Phys.* **2006**, *8*, 1624–1633.

- [50] M. M. Bhasin, J. H. McCain, B. V. Vora, T. Imai, P. R. Pujadó, *Appl. Catal. A* **2001**, *221*, 397–419.
- [51] J. Salmones, J.-A. Wang, J. A. Galicia, L. Balderas, G. Aguilar-Rios, *J. Mol. Catal. A* **2002**, *184*, 203–213.
- [52] H. Armendáriz, A. Guzmán, J. A. Toledo, M. E. Llanos, A. Vázquez, G. Aguilar-Rios, *Appl. Catal. A* **2001**, *211*, 69–80.
- [53] J. Llorca, N. Homs, J. León, J. Sales, J. L. G. Fierro, P. Ramirez de La Piscina, *Appl. Catal. A* **1999**, *189*, 77–86.
- [54] A. D. Ballarini, S. A. Bocanegra, A. A. Castro, S. R. de Miguel, O. A. Scelza, *Catal. Lett.* **2009**, *129*, 293–302.
- [55] S. A. Bocanegra, A. Guerrero-Ruiz, S. R. de Miguel, O. A. Scelza, *Appl. Catal. A* **2004**, *277*, 11–22.
- [56] G. Grubert, J. Rathousky, G. Schulz-Ekloff, M. Wark, A. Zukał, *Microporous Mesoporous Mater.* **1998**, *22*, 225–236.
- [57] E. V. Kondratenko, *Catal. Today* **2010**, *157*, 16–23.

Received: February 16, 2015

Revised: March 25, 2015

Published online on May 12, 2015